



The intercalation of bicyclic and tricyclic carboxylates into layered double hydroxides

Aamir I. Khan, Gareth R. Williams*, Gang Hu, Nicholas H. Rees, Dermot O'Hare**

Chemistry Research Laboratory, Department of Chemistry, University of Oxford, Mansfield Road, Oxford OX1 3TA, United Kingdom

ARTICLE INFO

Article history:

Received 26 May 2010

Received in revised form

10 September 2010

Accepted 26 September 2010

Available online 1 October 2010

Keywords:

Layered double hydroxide

Bicyclic/tricyclic carboxylate

Time-resolved diffraction

ABSTRACT

Twenty-four nanocomposites built from layered double hydroxides and bicyclic and tricyclic carboxylates have been synthesised for the first time. Eight carboxylates were successfully intercalated into $[\text{LiAl}_2(\text{OH})_6]\text{Cl} \cdot y\text{H}_2\text{O}$, $[\text{Ca}_2\text{Al}(\text{OH})_6]\text{NO}_3 \cdot y\text{H}_2\text{O}$, and $[\text{Mg}_2\text{Al}(\text{OH})_6]\text{NO}_3 \cdot y\text{H}_2\text{O}$, and the products fully characterised. Guest species incorporated include 1-adamantane carboxylate (1-AC) and 5-norbornene-2-endo-3-exo-dicarboxylate. In some cases, carbonate anions were co-intercalated with the organic guest, and in others poorly crystalline aluminium hydroxides formed as by-products. Sharper resonances were observed in the ^{13}C solid-state NMR spectra of the 1-AC intercalates than in the spectrum of pure 1-AC, suggesting increased order in the arrangement of the cyclic cages in the intercalates. Where possible, time-resolved *in situ* X-ray diffraction was employed to study the nanoscopic steps involved in the intercalation reactions. These investigations showed that the reactions are one-step processes, proceeding directly to the fully exchanged intercalate with no intermediate phases. The intercalation processes were found to be nucleation controlled.

© 2010 Elsevier Inc. All rights reserved.

1. Introduction

Layered double hydroxides (LDHs) are a family of layered materials containing positively charged layers and charge balancing anions located in the vacant space between the layers (see Fig. 1). The anions may be replaced *via* a facile anion exchange process. LDHs form with a variety of M^{2+} and M^{3+} cations (for instance $[\text{Mg}_2\text{Al}(\text{OH})_6]\text{NO}_3 \cdot y\text{H}_2\text{O}$ and $[\text{Ca}_2\text{Al}(\text{OH})_6]\text{NO}_3 \cdot y\text{H}_2\text{O}$), and also with Li^+ and Al^{3+} ($[\text{LiAl}_2(\text{OH})_6]\text{Cl} \cdot y\text{H}_2\text{O}$). These materials have a number of attractive properties, including shape-selective ion exchange [1–5], and catalytic activity [6–8]. Several recent reviews provide further information on the extensive anion-exchange chemistry of LDHs [8–11].

A significant number of organic carboxylates have been intercalated into a range of LDHs (see a comprehensive review by Carlino [12] for details). To date, however, the intercalation of bicyclic and tricyclic carboxylates has not been explored. These have a range of potential applications. For instance, derivatives of bicyclic and tricyclic carboxylates are used as drugs, and hence their intercalation could provide an important first step towards

advanced nanomaterials. Functionalised adamantane carboxylates are also thought to have an application as antiwear additives in lubricants, and in advanced polymers (e.g. nylon). Their intercalation is hence of interest: an LDH matrix releasing an antiwear agent at a controlled rate over time could be of use to ensure smooth lubrication over long periods of time without engineer intervention, and *in situ* polymerisation inside the LDH matrix could lead to new polymers with superior properties. On a more fundamental level, bicyclic and tricyclic carboxylates can have a range of different cage structures and functionalisation, and their intercalation should provide an insight into the interaction of LDH layers with bulky, low charged, anions. Furthermore, the intercalation of carboxylate species into $[\text{LiAl}_2(\text{OH})_6]\text{X} \cdot y\text{H}_2\text{O}$ has been shown to be interesting mechanistically, with ordered heterostructures observed as intermediates in some cases [13,14].

A fundamental study on the synthesis and characterisation of a series of novel bicyclic and tricyclic carboxylate intercalates of LDHs is reported here. Three LDHs were chosen for investigation: $[\text{LiAl}_2(\text{OH})_6]\text{Cl} \cdot y\text{H}_2\text{O}$ (because of its high crystallinity and known ability to form intermediates with carboxylate guests), $[\text{Mg}_2\text{Al}(\text{OH})_6]\text{NO}_3 \cdot y\text{H}_2\text{O}$ (owing to its widespread intercalation chemistry and biocompatibility), and $[\text{Ca}_2\text{Al}(\text{OH})_6]\text{NO}_3 \cdot y\text{H}_2\text{O}$ (as a result of its unusual metal coordination, with an expanded 7-fold coordination sphere about Ca). Twenty-four new intercalates have been synthesised and fully characterised. The intercalation reactions were investigated using *in situ* energy dispersive X-ray diffraction in order to probe reaction mechanisms, and also to determine kinetic parameters such as rate constants and activation energies.

* Correspondence to: School of Human Sciences, London Metropolitan University, 166–220 Holloway Road, London N7 8DB, United Kingdom. Fax: +44 207 133 4149.

** Corresponding author. Fax: +44 1865 272690.

E-mail addresses: g.williams@londonmet.ac.uk (G.R. Williams), dermot.ohare@chem.ox.ac.uk (D. O'Hare).

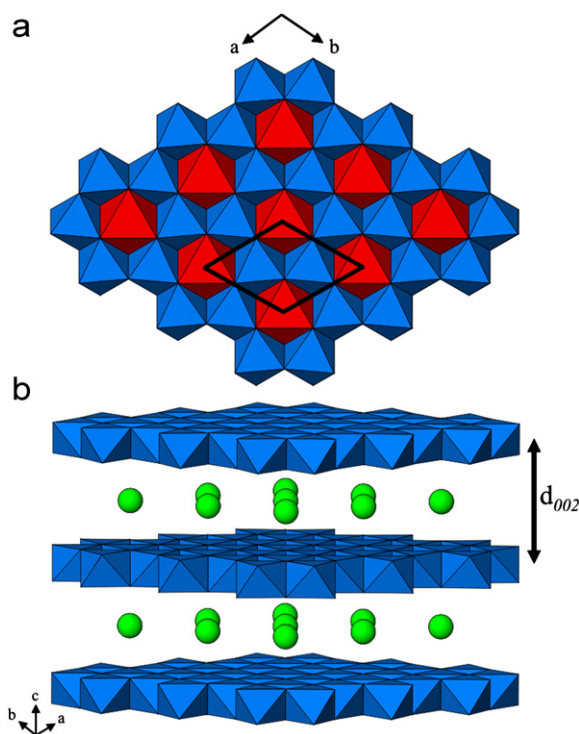


Fig. 1. The structure of the $[\text{LiAl}_2(\text{OH})_6]\text{Cl} \cdot y\text{H}_2\text{O}$ LDH. The layers comprise edge-sharing metal hydroxide octahedra. (a) The layers from above, with LiO_6 octahedra shown in red, and AlO_6 octahedra in blue. The unit cell is marked in black. (b) View showing the positive layers (blue) with anions (green) located in the interlayer space. H atoms are omitted for clarity. The $[\text{Mg}_2\text{Al}(\text{OH})_6]\text{NO}_3 \cdot y\text{H}_2\text{O}$ and $[\text{Ca}_2\text{Al}(\text{OH})_6]\text{NO}_3 \cdot y\text{H}_2\text{O}$ LDHs have similar structures, except that in the latter the Ca^{2+} ions have an expanded $3+3+1$ coordination sphere, in which they are bound to one interlayer water molecule in addition to six layer hydroxides. (For interpretation of the references to colour in this figure legend, the reader is referred to the web version of this article.)

2. Experimental details

2.1. Synthesis

$[\text{LiAl}_2(\text{OH})_6]\text{Cl} \cdot y\text{H}_2\text{O}$ (h-LiAl₂-Cl): Gibbsite $[\text{Al}(\text{OH})_3]$ was prepared by slowly dissolving 0.51 mol (13.77 g) of aluminium wire (99%, Aldrich) in a solution of 0.75 mol of NaOH (30 g) in 160 mL deionised H₂O at 80 °C. This reaction was undertaken in a Teflon[®] beaker, which was covered by a watch glass between each addition of the wire. Additional deionised H₂O was added in order to maintain a volume of 160 mL. The solution was allowed to cool and the filtrate placed in a sealed Naglene[®] plastic bottle and allowed to age at 80 °C for 3 days. A white solid was recovered by filtration, washed with water and acetone, dried in air, and ground. The hexagonal form of $[\text{LiAl}_2(\text{OH})_6]\text{Cl} \cdot y\text{H}_2\text{O}$ (h-LiAl₂-Cl) was then prepared by stirring a suspension of 0.09 mol of gibbsite (7 g) in 70 mL H₂O with a four-fold molar excess of LiCl at 90 °C for 3 days. Again, the solid obtained was recovered by filtration, washed with water and acetone, dried, and ground.

$[\text{Ca}_2\text{Al}(\text{OH})_6]\text{NO}_3 \cdot y\text{H}_2\text{O}$ (Ca₂Al-NO₃): was prepared using the coprecipitation method at room temperature as described by Millange et al. [15]. Typically, 17 g $\text{Ca}(\text{NO}_3)_2 \cdot 4\text{H}_2\text{O}$ and 11.7 g $\text{Al}(\text{NO}_3)_3 \cdot 9\text{H}_2\text{O}$ were dissolved in 80 mL of deionised water. This solution was added dropwise to a solution of 6.25 g NaOH and 9.1 g NaNO₃ in 44 mL deionised water and the mixture stirred vigorously during precipitation. Once addition was complete, the reaction mixture was stirred for 24 h at 80 °C. The resultant white solid was recovered by filtration, washed, and dried as described above.

$[\text{Mg}_2\text{Al}(\text{OH})_6]\text{NO}_3 \cdot y\text{H}_2\text{O}$ (Mg₂Al-NO₃): was prepared using the method described by Kaneyoshi and Jones [16]. 240 mL of a mixed metal nitrate solution containing 0.12 mol total metal content and with a Mg:Al ratio of 2:1 was added dropwise to 340 mL of aqueous solution containing 0.16 mol NaNO₃. The pH was adjusted initially to 10 by the addition of NaOH solution, and maintained at 10 throughout the reaction by the addition of 1 M NaOH. The reaction mixture was aged at 80 °C for 24 h. The resultant white solid was recovered by filtration, washed, and dried as described above.

Carboxylate salt solution preparation: All materials were supplied by Aldrich and Fluka. If possible, guests were purchased as sodium salts. If these were not available, sodium salts were typically prepared by stirring 1.4 mmol of the neutral guest (for a monoacid) or 0.7 mmol (for a diacid) with 1.4 mmol NaOH in 5 mL of H₂O. In either case, the carboxylate sodium salt in 5 mL H₂O was dissolved by the addition of a further 10 mL water.

Intercalation reactions were carried out in Young's ampoules containing the host, guest, deionised water, and a magnetic follower with pivot ring. The contents of the ampoule were stirred for the requisite time at a suitable temperature. Precise synthesis conditions for each intercalate are given in the Supporting Information (Table S1). The mixture was allowed to cool and filtered using a sintered glass frit. The powder was washed with water and acetone, and left to dry in air for approximately 1 h.

2.2. Characterisation

Elemental analysis: Elemental analyses were performed by the Analytical Services Department of the Inorganic Chemistry Laboratory, University of Oxford. C, H, and N contents of the samples were determined by quantitatively digesting the sample through an oxidative combustion. The samples were analysed for Li, Al, Mg, and Ca using inductively coupled plasma atomic emission spectroscopy.

Powder X-ray diffraction: Powder diffraction patterns were recorded on a Philips PW 1729 diffractometer or a PANalytical X'Pert Pro diffractometer. Both diffractometers utilise $\text{CuK}\alpha$ radiation ($\lambda(\text{K}\alpha 1) = 1.5406 \text{ \AA}$, $\lambda(\text{K}\alpha 2) = 1.5433 \text{ \AA}$, weighted average $\lambda = 1.5418 \text{ \AA}$) in reflection mode, at 40 kV and 30 mA for the Philips diffractometer and 40 kV and 40 mA for the PANalytical X'Pert Pro. For the Philips diffractometer, samples were mounted on aluminium plates. These show Bragg reflections of significant intensity, but the angular location of these reflections is such that there is no interference with the characterisation of products. The samples for the X'Pert Pro were mounted on stainless steel plates. No reflections from the stainless steel appeared in the d -spacing range of interest. This guarantees no interference with product characterisation.

Thermogravimetric analysis: Thermogravimetric analysis measurements were performed on a Rheometric Scientific STA-1500H instrument. The sample (approximately 30 mg) was mounted on a platinum crucible and heated at a rate of $10 \text{ }^\circ\text{C min}^{-1}$ between 20 and 1200 °C under a flow of argon.

Transmission electron microscopy: Electron micrographs were collected on a Jeol 4000FX 400 kV transmission electron microscope equipped with an Oxford Instruments 'Pentafet' Si/Li detector attached to a LINK eXL hardware system. Samples of the material to be analysed were suspended in absolute ethanol by means of an ultrasound bath, the mixture placed on a lacey carbon 200 mesh copper grid, and the solvent allowed to evaporate.

Infrared spectroscopy: IR spectra of the samples as KBr discs were recorded over the range $400\text{--}4000 \text{ cm}^{-1}$ on a MATTSON Galaxy Series Instrument 6020 FT-IR spectrometer. 16 scans were recorded with a scan resolution of 8 cm^{-1} .

Solid-state NMR: ^{13}C cross-polarization magic-angle-spinning (CP MAS) spectra were obtained on a Varian/Chemmagetics Infinity spectrometer at 100.6 MHz using 4.0 mm O.D. rotors containing 50 mg of sample. A MAS rate of 10 kHz was employed, and dry nitrogen utilised for all gas requirements. A cross-polarization sequence with a variable X-amplitude spin-lock pulse [17] and phase modulated proton decoupling was used. Typically, 4000 transients were acquired using a contact time of 3.0 ms, an acquisition time of 34 ms (1024 data points zero filled to 16 K) and a recycle delay of 20 s. All ^{13}C spectra were referenced to adamantane (the upfield methine resonance was taken to be at $\delta = 29.5$ ppm [18] on a scale where δ (TMS) = 0) as a secondary reference.

2.3. *In situ* time-resolved X-ray diffraction

Time-resolved energy-dispersive X-ray diffraction (EDXRD) experiments were performed on Station 16.4 of the UK Synchrotron Radiation Source (SRS) using an apparatus reported previously [11,14,19,20]. A solution containing a two-fold excess of the guest was added to 0.2 g of the LDH suspended in 3 mL deionised water. Both components had been pre-heated at the reaction temperature. Diffraction patterns were recorded until the intensity of the product reflections stopped increasing.

The program DLConvert was used to convert the data into a format suitable for an input into the Xfit peak profiling program. This latter program was used to fit Gaussian curves to the reflections observed experimentally. Reflection positions and widths were recorded and an automated Gaussian fitting routine used to obtain the areas of the Bragg reflections [21]. These values are subsequently converted to the extent of reaction at time t , $\alpha(t)$. This is defined as $\alpha(t) = I_{hkl}(t)/I_{hkl}(\text{max})$, where $I_{hkl}(t)$ is the area of a given reflection at time t , and $I_{hkl}(\text{max})$ is the maximum area of this reflection. Fluorescence lines were used as an internal standard against which to benchmark the integrated intensities. The Avrami-Erofe'ev model was then used to model the experimental data; details of this are given elsewhere [11,22,23].

3. Results

3.1. Synthesis of carboxylate intercalates

Full anion exchange of the initial interlayer anion of the h-LiAl₂-Cl, Mg₂Al-NO₃, and Ca₂Al-NO₃ materials for a range of bicyclic and tricyclic carboxylates was accomplished by simple ion-exchange. The compositions and interlayer separations of the new intercalates are summarised in Table 1. XRD data for the 1-adamantane carboxylate (1-AC) intercalate of h-LiAl₂-Cl (h-LiAl₂-1AC) are given in Fig. 2. The X-ray diffraction data for all the intercalates could be indexed on unit cells with a -parameters similar to those of the starting materials and expanded c -parameters. The unit cell of h-LiAl₂-Cl is illustrated in Fig. 1, and full details of the indexing are given in the Supporting Information (Tables S2–S4). It is clear from Fig. 2 that the (1 0 0) reflection does not change position or width upon intercalation, confirming that the arrangement of metal ions in the hydroxide layers in the LDH is unaffected. In contrast, the (0 0 l) reflections are noticeably broadened upon intercalation, as a result of the layers slipping laterally with respect to one another and inducing turbostratic disorder into the crystallites.

It can also be observed in Fig. 2 that there are two reflections which may not be indexed using the proposed unit cell. These are attributed to Al hydroxides (gibbsite [γ -Al(OH)₃] and boehmite [AlOOH]) which form concomitantly with the intercalation compound. Elemental analysis data is also consistent with the

formation of these phases (Table 1). This is a result of leaching of Li⁺ from the LDH layers. The number of bulky bicyclic or tricyclic carboxylate anions that can be accommodated in the interlayer region is lower than that of Cl[−] anions because of the larger size of the carboxylates. Therefore, metal cations are lost from the host structure in order to maintain charge neutrality. These results are in accordance with the work of other researchers; for instance, the deintercalation of Li⁺ ions from LiAl₂-X has previously been investigated, using an *in situ* X-ray diffraction [24]. The same features of broadening 00 l reflections and the formation of poorly crystalline Al hydroxides can be observed for Ca₂Al-1AC and Mg₂Al-1AC, and indeed for all the bicyclic and tricyclic carboxylates.

From the elemental analysis data (see Table 1 for a summary), it can be inferred that some of the intercalates contain carbonate anions. The presence of carbonate is confirmed by the occurrence of a characteristic band of the carbonate anion at ca. 1375 cm^{−1} in the IR spectra of these intercalates. Some carbonate will be present in the water used as the reaction solvent, and some CO₂ from the air may also dissolve to produce additional carbonate. The intercalation of carbonate is very favourable owing to its small size and high charge, and replacement of carbonate ions in LDHs is very difficult. Hence, despite the significant excess of the organic carboxylate in the reaction solution, carbonate incorporation is common in the intercalation chemistry of LDHs.

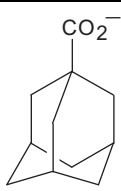
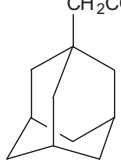
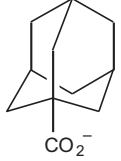

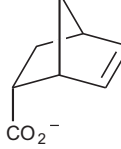
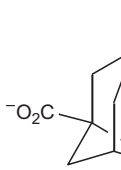
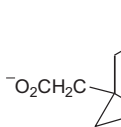
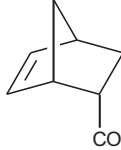
3.2. Orientation of guests

The space available to the guest anions in the interlayer region can be calculated approximately by subtracting the layer thickness of 4.8 Å from the interlayer spacings observed by X-ray diffraction [25]. The most feasible arrangement of guest anions in the interlayer region will be that which maximises host–guest and guest–guest interactions. Comparison of the end-to-end distance of the 1-AC anion (calculated from single crystal X-ray diffraction data to be 7.0 Å, including van der Waals radii [26]) with the d_{002} value for h-LiAl₂-1AC (20.2 Å) suggests that this guest adopts a bilayer arrangement in the interlayer region. This arrangement results in the maximisation of electrostatic interactions and hydrogen bonding between the metal hydroxide sheets and the carboxylate groups. The aliphatic portion of the guest remains in the centre of the gallery, forming a hydrophobic region. This arrangement is depicted in Fig. 3(a). Similar results have been reported for fatty acid intercalates [27]. The d_{002} values for the 1-AC intercalates of Mg₂Al-NO₃ and Ca₂Al-NO₃ are 20.0 and 20.2 Å, respectively, almost identical to the h-LiAl₂-1AC material, and also consistent with the bilayer formation.

In the case of 1,3-adamantane dicarboxylate (1,3-ADC), comparison of d_{002} of h-LiAl₂-1,3ADC (15.4 Å) with the size of the anion (8.8 Å) implies the formation of a monolayer in the interlayer region. Both carboxylate groups of each guest anion are able to bond to adjacent layers resulting in the most favourable host–guest interactions with such a monolayer arrangement [28]. A schematic representation of the orientation of 1,3-ADC in h-LiAl₂-1,3ADC is shown in Fig. 3(b). Again, it can be seen that the d_{002} values for Mg₂Al-1,3ADC and Ca₂Al-1,3ADC (16.8 and 14.2 Å, respectively) are similar to the h-LiAl₂-1,3ADC distance, also consistent with the monolayer formation.

The interlayer spacings of the remainder of the intercalation compounds of all three LDHs are consistent with the formation of a bilayer (carboxylates) or a monolayer (dicarboxylates) in the interlayer region. The layer separations of the 1-adamantane acetate (1-AA) intercalates are larger than those of the 1-AC intercalates as a result of the greater bulk of 1-AA: 1-AA has a CH₂ group between the carbonate group and the cyclic cage which 1-AC does not, resulting in the bilayer taking up more

Table 1The compositions and interlayer spacings of the bicyclic and tricyclic carboxylate intercalates. 'A' represents $[\text{Al}(\text{OH})_3]$.

Carboxylate	Structure	Intercalation compound ^a	d_{001} (Å) ^b
1-Adamantane carboxylate (1-AC)		$[\text{LiAl}_2(\text{OH})_6][1\text{-AC}] \cdot 3.50\text{H}_2\text{O} [\text{A}]_{0.1}$ $[\text{Mg}_2\text{Al}(\text{OH})_6][1\text{-AC}] \cdot 2.90\text{H}_2\text{O} [\text{A}]_{0.38}$ $[\text{Ca}_2\text{Al}(\text{OH})_6][1\text{-AC}]_{0.85}(\text{CO}_3)_{0.08} \cdot 2.68\text{H}_2\text{O} [\text{A}]_{0.55}$	20.2 20.0 20.2
1-Adamantane acetate (1-AA)		$[\text{LiAl}_2(\text{OH})_6][1\text{-AA}] \cdot 3.58\text{H}_2\text{O} [\text{A}]_{0.28}$ $[\text{Mg}_2\text{Al}(\text{OH})_6][1\text{-AA}]_{0.81}(\text{CO}_3)_{0.09} \cdot 2.57\text{H}_2\text{O}$ $[\text{Ca}_2\text{Al}(\text{OH})_6][1\text{-AA}] \cdot 4.63\text{H}_2\text{O} [\text{A}]_{0.63}$	21.5 21.9 21.5
3-Noradamantane carboxylate (3-NC)		$[\text{LiAl}_2(\text{OH})_6][3\text{-NC}] \cdot 2.90\text{H}_2\text{O} [\text{A}]_{0.66}$ $[\text{Mg}_2\text{Al}(\text{OH})_6][3\text{-NC}]_{0.78}(\text{CO}_3)_{0.11} \cdot 2.38\text{H}_2\text{O}$ $[\text{Ca}_2\text{Al}(\text{OH})_6][3\text{-NC}] \cdot 1.32\text{H}_2\text{O} [\text{A}]_{0.69}$	18.9 19.2 20.3
Norbornane-2-carboxylate (N-2C)		$[\text{LiAl}_2(\text{OH})_6][\text{N-2C}] \cdot 3.80\text{H}_2\text{O} [\text{A}]$ $[\text{Mg}_2\text{Al}(\text{OH})_6][\text{N-2C}]_{0.76}(\text{CO}_3)_{0.12} \cdot 1.92\text{H}_2\text{O}$ $[\text{Ca}_2\text{Al}(\text{OH})_6][\text{N-2C}]_{0.50}(\text{CO}_3)_{0.25} \cdot 2.62\text{H}_2\text{O} [\text{A}]_{0.77}$	18.7 16.8 15.8
5-Norbornene-2-carboxylate (5-NC)		$[\text{LiAl}_2(\text{OH})_6][5\text{-NC}] \cdot 3.00\text{H}_2\text{O} [\text{A}]_{0.76}$ $[\text{Mg}_2\text{Al}(\text{OH})_6][5\text{-NC}]_{0.56}(\text{CO}_3)_{0.22} \cdot 2.17\text{H}_2\text{O} [\text{A}]_{0.40}$ $[\text{Ca}_2\text{Al}(\text{OH})_6][5\text{-NC}]_{0.55}(\text{CO}_3)_{0.23} \cdot 2.32\text{H}_2\text{O} [\text{A}]_{0.90}$	18.3 17.5 15.4
1,3-Adamantane dicarboxylate (1,3-ADC)		$[\text{LiAl}_2(\text{OH})_6][1,3\text{-ADC}]_{0.50} \cdot 4.48\text{H}_2\text{O} [\text{A}]_{0.92}$ $[\text{Mg}_2\text{Al}(\text{OH})_6][1,3\text{-ADC}]_{0.40}(\text{CO}_3)_{0.10} \cdot 3.02\text{H}_2\text{O}$ $[\text{Ca}_2\text{Al}(\text{OH})_6][1,3\text{-ADC}]_{0.40}(\text{CO}_3)_{0.10} \cdot 4.12\text{H}_2\text{O} [\text{A}]_{0.80}$	15.3 16.8 14.2
1,3-Adamantane diacetate (1,3-ADA)		$[\text{LiAl}_2(\text{OH})_6][1,3\text{-ADA}]_{0.50} \cdot 3.29\text{H}_2\text{O} [\text{A}]_{0.45}$ $[\text{Mg}_2\text{Al}(\text{OH})_6][1,3\text{-ADA}]_{0.37}(\text{CO}_3)_{0.13} \cdot 2.55\text{H}_2\text{O}$ $[\text{Ca}_2\text{Al}(\text{OH})_6][1,3\text{-ADA}]_{0.50} \cdot 4.00\text{H}_2\text{O} [\text{A}]$	16.1 16.9 16.1
5-Norbornene-2-endo-3-exo-dicarboxylate (5-NDC)		$[\text{LiAl}_2(\text{OH})_6][5\text{-NDC}]_{0.50} \cdot 3.80\text{H}_2\text{O} [\text{A}]_{0.86}$ $[\text{Mg}_2\text{Al}(\text{OH})_6][5\text{-NDC}]_{0.42}(\text{CO}_3)_{0.08} \cdot 2.48\text{H}_2\text{O}$ $[\text{Ca}_2\text{Al}(\text{OH})_6][5\text{-NDC}]_{0.36}(\text{CO}_3)_{0.13} \cdot 3.27\text{H}_2\text{O} [\text{A}]_{0.83}$	11.8 11.8 11.5

^a In a number of cases, reflections corresponding to both $\text{Al}(\text{OH})_3$ and AlOOH were observed in the XRD patterns of the intercalates; we were unable to determine the relative proportions of each, and hence have calculated all formulae based on only an $\text{Al}(\text{OH})_3$ impurity being present. Any error in the formula introduced by this approximation will be small and will not significantly affect the formulae of the intercalates, in which we are most interested.

^b d_{002} is given for intercalates of $\text{LiAl}_2\text{-Cl}$ and $\text{Ca}_2\text{Al-NO}_3$; d_{003} for intercalates of $\text{Mg}_2\text{Al-NO}_3$.

space, and a larger d_{002} for the former. Comparing the data for 3-noradamantane carboxylate (3-NC) and 1-AC, the h- $\text{LiAl}_2\text{-Cl}$ and $\text{Mg}_2\text{Al-NO}_3$ intercalates of 3-NC have a d -spacing of *ca.* 1 Å less than those of the 1-AC. This is a result of the *endo* carboxylate group being 'nested' inside the basal ring for 3-NC, whereas for 1-AC it is in the apical position; therefore, the end-to-end length of the latter anion is longer. In contrast, the d -spacings for the $\text{Ca}_2\text{Al-3NC}$ and $\text{Ca}_2\text{Al-1AC}$ intercalates are almost identical,

presumably as a result of the expanded Ca coordination sphere (7 *cf.* 6 for Mg and Li). The introduction of a second carboxylate group in 1,3-ADC (*cf.* 1-AC) causes the d -spacing to be reduced by 3.2–6 Å as a result of the two carboxylates being able to bind to opposite layers and form a monolayer as opposed to the bilayer formed with 1-AC. An analogous reduction of d -spacing (4.4–5.4 Å) is seen when moving from 1-adamantane acetate to 1,3-adamantane diacetate (1,3-ADA), for the same reasons. The 1,3-ADA

intercalates have slightly larger d -spacings than the 1,3-ADC intercalates (by 0.1–1.9 Å) as a result of the larger steric bulk of 1,3-ADA.

There are no clear trends in d -spacing for the norbornene-2-carboxylate (*N*-2C) and 5-norbornene-2-carboxylate intercalates (5-NC), and so for these bicyclics the *endo* or *exo* position of the carboxylate group does not have a straightforward effect on orientation. The introduction of a second carboxylate group in 5-norbornene-2-*endo*-3-*exo*-dicarboxylate leads to a reduction in interlayer spacing of 3.5–6.9 Å (cf. *N*-2C and 5-NC) as a result of the two carboxylate groups being able to bind to opposite layers (in a monolayer), whereas the mono-carboxylates can only bind to one layer and must form a bilayer.

3.3. Infrared spectroscopy

IR spectra of h-LiAl₂-Cl, 1-AA, and h-LiAl₂-1AA are displayed in Fig. 4. The IR spectrum of h-LiAl₂-Cl is typical of that for hydroxalclites [29,30]. The absorption at 3450 cm⁻¹ corresponds to stretching vibrations of the OH groups of the layers and the absorption at 1650 cm⁻¹ is attributed to the bending vibration of the interlayer water. The spectrum of the intercalate contains bands characteristic of the 1-AA anion as well as of the LDH. The absorptions at 2902 and 2846 cm⁻¹ correspond, respectively, to the

asymmetric and symmetric stretches of the 1-AA CH₂ unit. The bands at 1536 and 1404 cm⁻¹ are attributed to the asymmetric and symmetric stretching vibrations of the carboxylate group. The shift of the carboxylate bands of 1-AA (1710 and 1650 cm⁻¹) to lower wavenumber upon intercalation is a result of the weakening of these bonds owing to the interactions between the carboxylate group and the positively charged LDH layers. The region between 1450 and 500 cm⁻¹ contains bands corresponding to stretching and bending vibrations of the C–C and C–O bonds. This similarity of the IR spectrum of the 1-AA guest and the intercalate confirms the intercalation of the intact 1-AA guest.

Analogous results are obtained for the remaining h-LiAl₂-Cl intercalates, and also for all the Ca₂Al-NO₃ and Mg₂Al-NO₃ intercalates. In each case, vibrations characteristic of the guest are clearly visible in the IR spectra, demonstrating an intact intercalation of the guest anion. Where significant carbonate incorporation is suggested by an elemental analysis, this can also be seen in the spectra (at ca. 1375 cm⁻¹).

3.4. Transmission electron microscopy

Transmission electron microscopy (TEM) images of h-LiAl₂-Cl and its 1-AA intercalate (h-LiAl₂-1AA) are depicted in Fig. 5. The layered

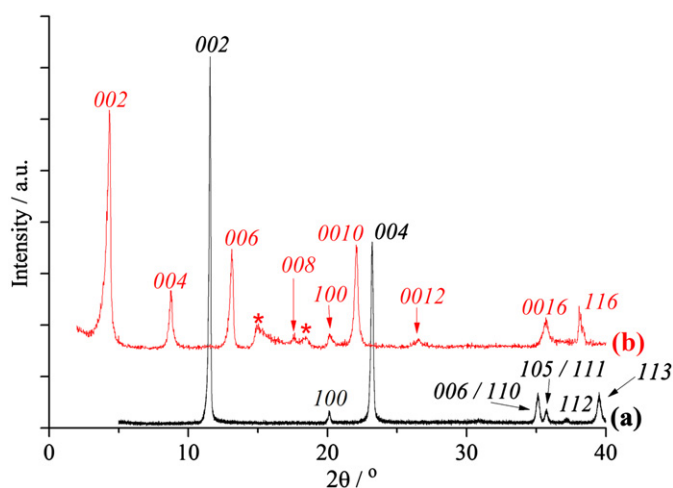


Fig. 2. XRD data for (a) h-LiAl₂-Cl and (b) h-LiAl₂-1AC, with reflections indexed. Reflections marked * correspond to an Al hydroxide.

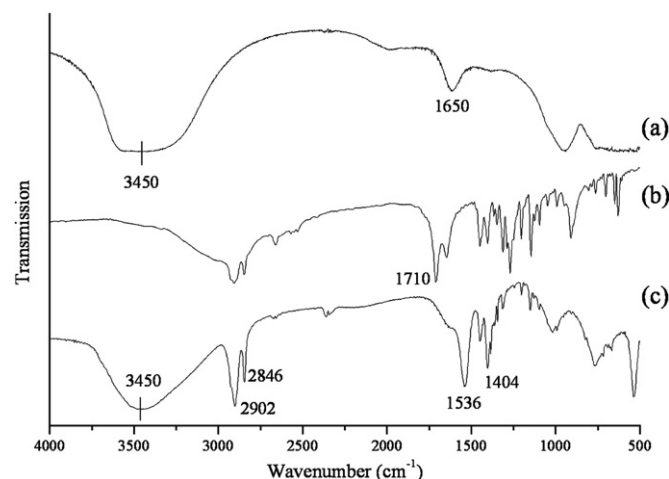


Fig. 4. IR spectra of (a) h-LiAl₂-Cl, (b) 1-AA, and (c) h-LiAl₂-1AA.

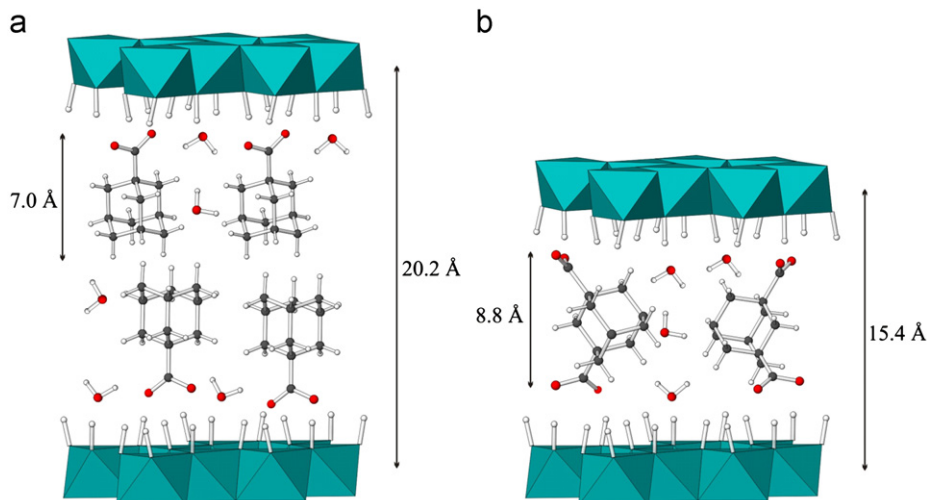


Fig. 3. Schematic representation showing the likely arrangement of (a) 1-AC and (b) 1,3-ADC in their h-LiAl₂-Cl intercalates.

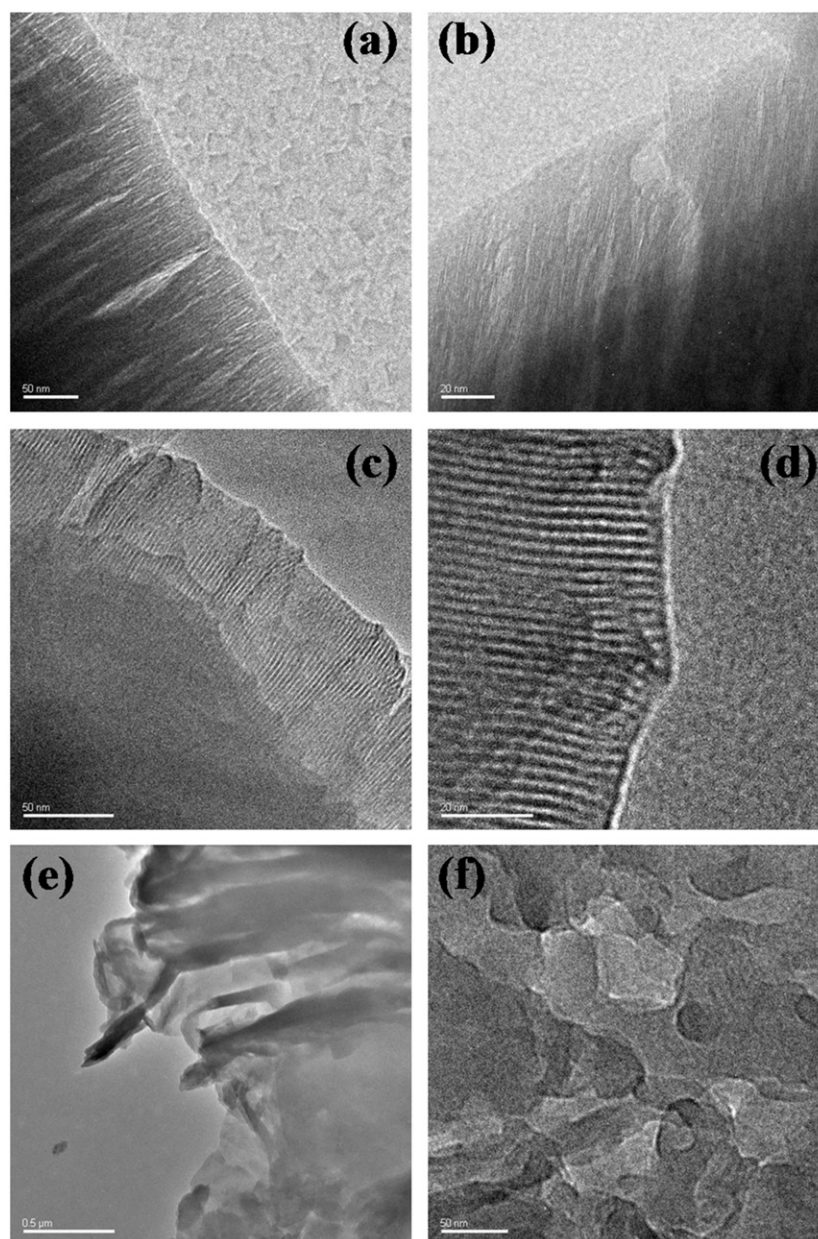


Fig. 5. TEM images showing: (a, b) h-LiAl₂-Cl; (c, d) h-LiAl₂-1AA; and (e, f) the Al hydroxide impurity, which forms concomitantly with the 1-AA intercalate.

nature of h-LiAl₂-Cl can be seen clearly in Fig. 5(a) and (b). The layers in the intercalate are also visible; comparisons of Fig. 5(a) with (c) and (b) with (d) clearly show an increase in layer separation as a result of the intercalation of 1-AA. Calculation of the interlayer spacing of the intercalate using the scale in Fig. 5(d) gives a value of approximately 22 Å, in good agreement with the X-ray diffraction data.

Largely amorphous Al hydroxide is clearly visible in the TEM images in Fig. 5(e) and (f). This concurs with the X-ray diffraction and elemental analysis data. TEM was also employed to study a selection of the other intercalates, both of h-LiAl₂-Cl and also of Mg₂Al-NO₃ and Ca₂Al-NO₃. The layered nature of the materials can be seen in the micrographs, as can Al hydroxide phases in some cases.

3.5. Thermogravimetric analysis

Thermogravimetric analysis (TGA) was performed on the intercalates over the temperature range 20–1200 °C. TGA allows the determination of the amount of co-intercalated water present and the

nature of the decomposition products of the compound. A typical TGA plot (that of h-LiAl₂-1AA) is shown in Fig. 6. The first mass loss (ca. 15%) is due to the loss of co-intercalated water from [LiAl₂(OH)₆][1-AA] · 3.58H₂O[Al(OH)₃]_{0.28}, leading to the formation of [LiAl₂(OH)₆][1-AA][Al(OH)₃]_{0.28}. This is followed by further loss of water (approximately 13%) owing to the dehydration of the layers. The final mass loss, of approximately 42%, corresponds to the decomposition of the guest and results in the formation of lithiated alumina. Similar three-stage mass loss was observed for the remaining carboxylate intercalates of all three LDHs, and is typical of LDH compounds.

3.6. Nuclear magnetic resonance

Solid state magic-angle spinning nuclear magnetic resonance was employed to investigate the 1-AC intercalates of h-LiAl₂-Cl and Ca₂Al-NO₃. Spectra are provided in Fig. 7, and germane parameters are summarised in Table 2. It can be seen that the chemical shifts observed are in very good agreement with

literature values obtained in CDCl_3 [31]. The spectra of the 1-AC intercalates are very similar to that of 1-AC, confirming that the organic guests are intercalated intact into the LDHs.

While the spectra of $\text{h-LiAl}_2\text{-1AC}$ and $\text{Ca}_2\text{Al-1AC}$ show peaks at approximately the same chemical shifts as the 1-AC starting material, the resonances are broader in the spectrum of 1-AC than in those of its intercalates. There will be significant disorder in the packing of individual molecules in the solid 1-AC, which produces a relatively high chemical shift anisotropy and therefore broad peaks. In contrast, in the intercalates, the carboxylate group will be tightly bound to the LDH layers by electrostatic and H-bonding interactions. This reduces the freedom of movement available to the anions, and hence they are more ordered than in pure 1-AC. The chemical shift anisotropy is thereby reduced, resulting in narrower peaks being observed in the intercalates' NMR spectra.

It is also clear from the NMR data that there is a small difference in the chemical shift of the carboxylate groups between 1-AC and the intercalation compounds. This is because the carboxylate group is protonated in pure 1-AC and deprotonated in $\text{h-LiAl}_2\text{-1AC}$ and $\text{Ca}_2\text{Al-1AC}$.

3.7. Time-resolved X-ray diffraction studies

Attempts were made to study the intercalation of the bi- and tricyclic carboxylates using *in situ* time-resolved energy-dispersive

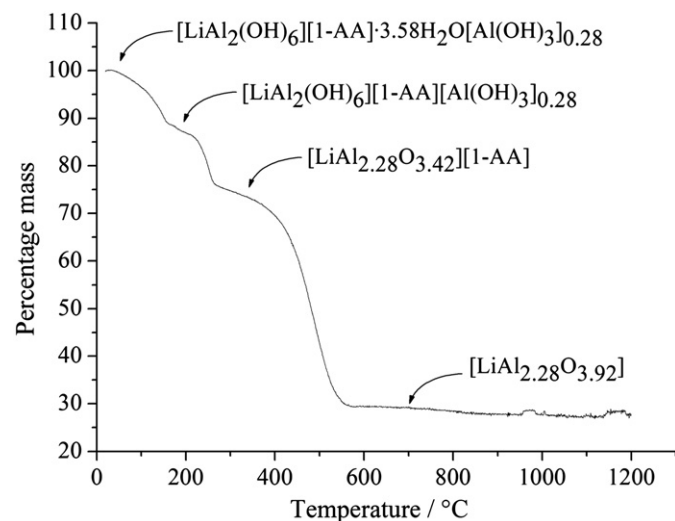


Fig. 6. TGA plot for $\text{h-LiAl}_2\text{-1AA}$.

XRD (EDXRD). The intercalation of the norbornane based structures into $\text{h-LiAl}_2\text{-Cl}$ and $\text{Ca}_2\text{Al-NO}_3$ and intercalation of all guests into $\text{Mg}_2\text{Al-NO}_3$ were found to be too rapid to monitor accurately. In other cases, poor crystallinity of the product phase precluded a detailed analysis. However, it was possible to study successfully six of the intercalation reactions using this technique.

3.7.1. Intercalation of 1-adamantane carboxylate into $\text{h-LiAl}_2\text{-Cl}$

The temperature dependence of the intercalation of 1-AC was investigated over the range 40–60 °C. A three-dimensional plot for the reaction at 40 °C showing the growth of the (002) Bragg reflection of the first stage intercalate is shown in Fig. 8. In all cases, the reactions proceeded directly from the host to the first stage intercalate: no intermediates were observed. Extent of reaction ($\alpha = I_{hkl}(t)/I_{hkl}(\text{max})$) vs. time plots are given in Fig. 9(a). It is clear that the rate of the reaction has a marked temperature dependence. Plots of the extent of reaction against reduced time ($t/t_{0.5}$) were found to be superimposable within an experimental error at the temperatures studied (Fig. 9(b)), showing that the mechanism for intercalation is consistent over this temperature range.

The Avrami–Erofe'ev equation has been successfully fitted to each data set. This equation takes the form $[-\ln(1-\alpha)]^{1/n} = k(t-t_0)$, where α is the extent of reaction; the exponent n provides information on the reaction mechanism; k is the rate constant; and t_0 is the induction time [23]. The value of the Avrami exponents (n) obtained was found to be in the range 1.53–1.85, and setting of $n=1.5$ gives a good fit to all the experimental data sets (see Fig. 9(a)). This corresponds to a situation in which there is 2D diffusion control following deceleratory nucleation. In these

Table 2

A summary of the NMR data for the 1-adamantane carboxylate intercalates $\text{h-LiAl}_2\text{-1AC}$ and $\text{Ca}_2\text{Al-1AC}$ (all given to 3s.f.). Literature values are taken from Ref. [31]. Please see Fig. 7 for the carbon atom numbering scheme.

		Cn				
		C1	C2, 8, 10	C4, 6, 9	C3, 5, 7	CO ₂ ⁻
Literature	δ (ppm)	42.9	40.5	37.2	29.0	189
1-AC	δ (ppm)		41.4	37.7	29.1	184
	$\Delta\nu_{1/2}$ (Hz)		135	989	528	126
$\text{h-LiAl}_2\text{-1AC}$	δ (ppm)	42.8	41.0	37.9	29.8	187
	$\Delta\nu_{1/2}$ (Hz)	76.9	120	504	86.4	146
$\text{Ca}_2\text{Al-1AC}$	δ (ppm)	42.9	41.9/40.6	39.8/37.9/35.7	29.4	106
	$\Delta\nu_{1/2}$ (Hz)	76.3	143/117	146/245/604	188	128

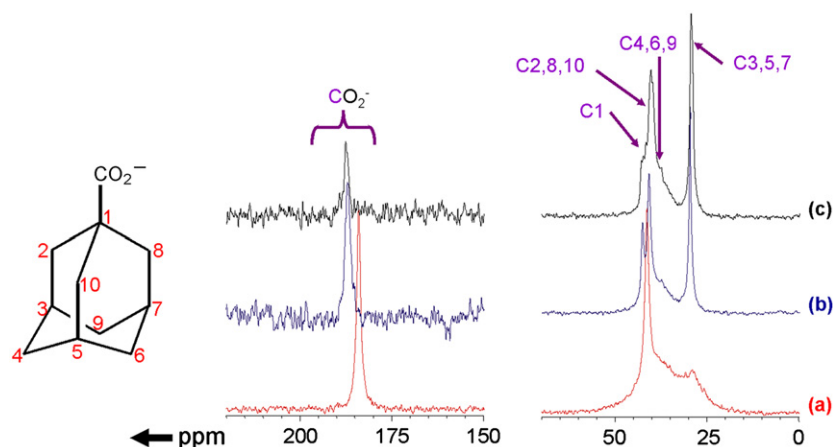


Fig. 7. Solid-state ^{13}C NMR data for (a) 1-AC; (b) $\text{h-LiAl}_2\text{-1AC}$; and (c) $\text{Ca}_2\text{Al-1AC}$.

circumstances, the nucleation sites (*i.e.* the layer edges) are activated one by one as the reaction proceeds. If a perfect host lattice (without defects) is considered, then there are a given number of identical nucleation sites, s , at the crystalline faces. The possibility of nucleation occurring at each site is the same, p . Therefore, the nucleation rate is $p \times s$. As the reaction proceeds, some of the layers become filled. The edges of these layers are no longer potential nucleation sites, and so as the reaction progresses, s decreases, and hence the nucleation rate falls.

The values of n and k may be calculated using the Sharp–Hancock equation. This takes the form $\ln(-\ln(1-\alpha)) = n \ln k + n \ln t$, and a graph of $\ln(-\ln(1-\alpha))$ vs. $\ln t$ should be linear if the Avrami–Erofe'ev model is valid. n can be directly calculated from the gradient of the graph, and k from the intercept. The validity of setting $n=1.5$ for the intercalation of 1-AC into h-LiAl₂-Cl was confirmed by Sharp–Hancock analysis. At each temperature, the Sharp–Hancock plots were found to be linear, as shown in Fig. 10, verifying that the Avrami–Erofe'ev model provides a reasonable description of this system. The kinetic parameters calculated from the plots are listed in Table 3. These allow the activation energy for the intercalation of 1-AC into h-LiAl₂-Cl to be calculated using the Arrhenius expression,

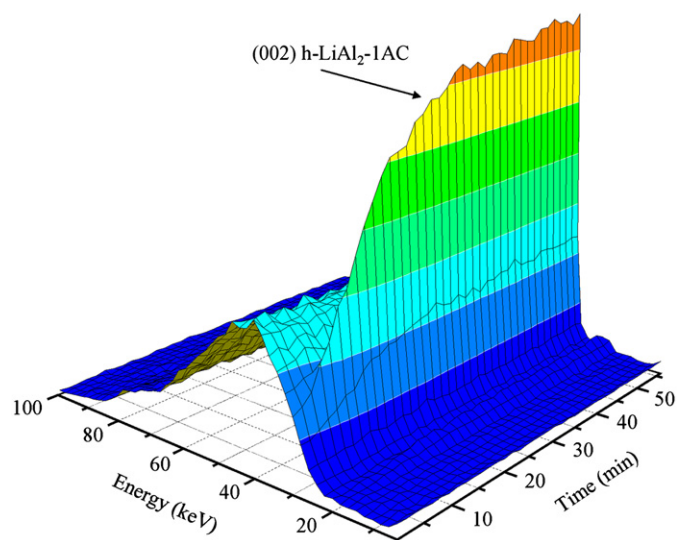


Fig. 8. Three-dimensional plot of the diffraction data collected for the intercalation of 1-AC into h-LiAl₂-Cl at 40 °C, showing the (0 0 2) Bragg reflection of h-LiAl₂-1AC increasing with time.

$k = Ae^{-E_a/RT}$. A plot of $\ln k$ against $-1/T$ is given in Fig. 11, and yields an activation energy of 68.4 ± 4.7 kJ mol⁻¹. This value is consistent with a nucleation controlled reaction mechanism, as diffusion controlled reactions typically have much lower activation energies of the order of 15 kJ mol⁻¹.

3.7.2. Other intercalation reactions

The intercalations of 1-AA, 1,3-ADC, and 1,3-ADA into h-LiAl₂-Cl and of 1-AA and 1,3-ADC into Ca₂Al-NO₃ were also successfully probed using EDXRD. Complete data for these processes is given in the Supporting Information, and a summary is provided in Table 4. In the majority of cases, the values of n are between 1 and 2

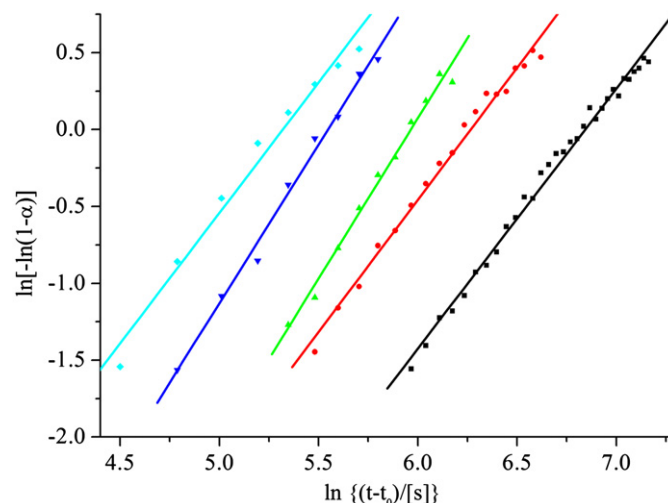


Fig. 10. Sharp–Hancock plots for the intercalation of 1-AC into h-LiAl₂-Cl at 40 °C (■), 45 °C (●), 50 °C (▲), 55 °C (▼), and 60 °C (◆).

Table 3

The kinetic parameters obtained from Sharp–Hancock analysis of the intercalation of 1-adamantane carboxylate into h-LiAl₂-Cl.

Temperature (°C)	n	k (10 ⁻³ s ⁻¹)	$t_{0.5}$ (s)
40	1.69 ± 0.03	1.07 ± 0.04	735
45	1.72 ± 0.05	1.90 ± 0.16	480
50	1.73 ± 0.09	2.50 ± 0.18	315
55	1.86 ± 0.09	3.90 ± 0.27	210
60	1.76 ± 0.10	5.00 ± 0.35	150

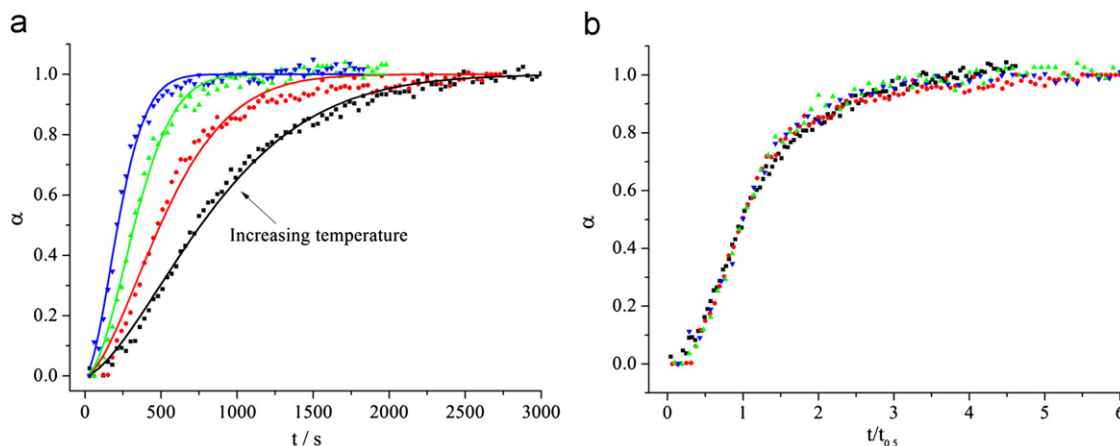


Fig. 9. (a) Extent of reaction (α) plotted against time for the intercalation of 1-AC into h-LiAl₂-Cl at 40 °C (■), 45 °C (●), 50 °C (▲), and 55 °C (▼). Lines show fits of the Avrami–Erofe'ev model with $n=1.5$ to the observed data. (b) Plots of extent of reaction against reduced time at the same temperatures. Data at 60 °C are omitted for clarity.

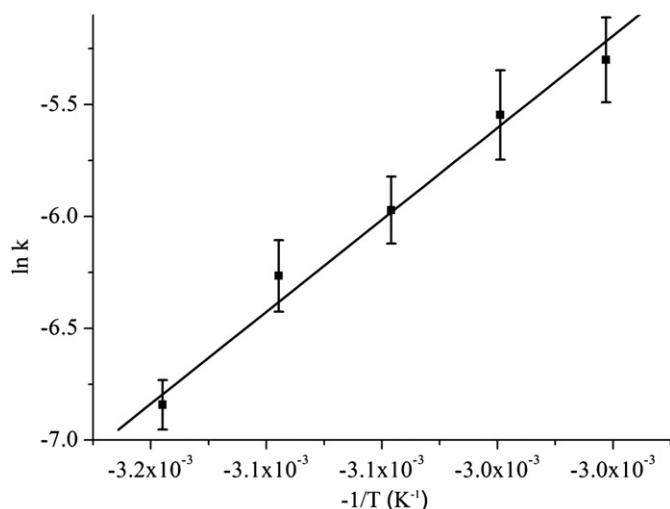


Fig. 11. Arrhenius plot for the intercalation of 1-AC into h-LiAl₂-Cl.

Table 4

Summary of the *in situ* diffraction data collected for the intercalation of bicyclic and tricyclic carboxylates.

Host	Guest	<i>n</i>	<i>E_a</i> (kJ mol ^{−1})	Complete data given in
h-LiAl ₂ -Cl	1-AA	1.58–1.85	82.8 ± 6.2	Figs. S1, S2; Table S5
	1,3-ADC	1.02–1.76	103.2 ± 4.9	Fig. S3; Table S6
	1,3-ADA	0.87–1.02	64.5 ± 1.2	Figs. S4, S5; Table S7
Ca ₂ Al-NO ₃	1-AA	1.34–1.59	40.6 ± 3.7	Figs. S6, S7; Table S8
	1,3-ADC	0.89–1.09	72.8 ± 5.0	Figs. S8, S9; Table S9

implying that the reactions are 2D diffusion controlled following deceleratory nucleation, as described in Section 3.7.1. The intercalations of 1,3-ADA into h-LiAl₂-Cl and 1,3-ADC into Ca₂Al-NO₃ are exceptional, and nucleation is instantaneous in these cases. This means that all nucleation sites are activated at the start of the reaction.

All of the calculated activation energies are consistent with a nucleation controlled reaction, lying in the range 40–104 kJ mol^{−1}. The activation energy for the intercalation of 1-AA into h-LiAl₂-Cl is higher than that for the intercalation of 1-AC (82.8 ± 6.2 kJ mol^{−1} for the former, *cf.* 68.4 ± 4.7 kJ mol^{−1} for the latter) owing to the increased steric bulk of the 1-AA anion. The activation energy for intercalation of the dicarboxylate 1,3-ADC into h-LiAl₂-Cl is larger than that for the mono-carboxylate 1-AC (103.2 ± 4.9 kJ mol^{−1} *cf.* 68.4 ± 4.7 kJ mol^{−1}), presumably as a result of the more highly charged dicarboxylate guest being more strongly solvated when in solution. In contrast, the activation energy for the intercalation of 1,3-ADA into h-LiAl₂-Cl is lower than the value for the intercalation of 1-AA. This differing behaviour can be attributed to the different mechanisms of reaction. The intercalation of 1-AA occurs with deceleratory nucleation, whereas that of 1,3-ADA proceeds with instantaneous nucleation.

4. Conclusions

A range of bicyclic and tricyclic carboxylates have been intercalated into [LiAl₂(OH)₆]Cl · yH₂O, [Ca₂Al(OH)₆]NO₃ · yH₂O and [Mg₂Al(OH)₆]NO₃ · yH₂O for the first time, and the products fully characterised. In some cases, carbonate anions were co-intercalated with the organic guest, and in others poorly crystalline aluminium hydroxides were observed to form as by-products. Twenty-four new intercalates are reported. The

1-adamantane carboxylate (1-AC) intercalates were studied by solid-state NMR: it was found that the intercalates exhibited sharper resonances than pure 1-AC, suggesting greater order in the arrangement of the cyclic cages in the intercalate. Unfortunately, it was only possible to study six of the 24 intercalation reactions by time-resolved *in situ* X-ray diffraction studies; those reactions that could be successfully studied are one-step processes, proceeding directly to the fully exchanged intercalate with no intermediate phases observed. The intercalation processes were found to be nucleation controlled. Future work will be focussed on studying how easily the bicyclic and tricyclic carboxylates can be displaced by other anions. Alternative reaction routes (*e.g.* coprecipitation or hydrothermal synthesis) will also be explored in the hope of avoiding Al hydroxide phases forming concomitantly with the intercalation compounds.

Acknowledgments

The authors thank the EPSRC for funding; the Science and Technology Facilities Council for access to the UK Synchrotron Radiation Source; and Dr. Dave Taylor and Mr. Alfie Nield for technical assistance on Station 16.4.

Appendix A. Supplementary information

Supplementary data associated with this article can be found in the online version at doi:10.1016/j.jssc.2010.09.036.

References

- [1] A.M. Fogg, J.S. Dunn, S.G. Shyu, D.R. Cary, D. O'Hare, Chem. Mater. 10 (1998) 351.
- [2] A.M. Fogg, V.M. Green, H.G. Harvey, D. O'Hare, Adv. Mater. 11 (1999) 1466.
- [3] L. Lei, F. Millange, R.I. Walton, D. O'Hare, J. Mater. Chem. 10 (2000) 1881.
- [4] L. Lei, R.P. Vijayan, D. O'Hare, J. Mater. Chem. 11 (2001) 3276.
- [5] R. Allmann, Chemica 24 (1970) 99.
- [6] F. Cavini, E. Trifiro, A. Vaccari, Catal. Today 11 (1991) 173.
- [7] M. Chibwe, J.B. Valim, W. Jones, NATO ASI Ser., Ser. C 400 (1993) 191.
- [8] A.I. Khan, D. O'Hare, J. Mater. Chem. 12 (2002) 3191.
- [9] V. Rives, Layered Double Hydroxides: Present and Future, Nova Science Publishers Inc., New York, 2001, 439 pp.
- [10] S.M. Auerbach, K.A. Carrado, P.K. Dutta (Eds.), Handbook of Layered Materials, Marcel Dekker, New York, 2004, p. 646.
- [11] G.R. Williams, A.I. Khan, D. O'Hare, Struct. Bonding 119 (2006) 161.
- [12] S. Carlino, Solid State Ionics 98 (1997) 73.
- [13] A.M. Fogg, J.S. Dunn, D. O'Hare, Chem. Mater. 10 (1998) 356.
- [14] G.R. Williams, D. O'Hare, Chem. Mater. 17 (2005) 2632.
- [15] F. Millange, R.I. Walton, L. Lei, D. O'Hare, Chem. Mater. 12 (2000) 1990.
- [16] M. Kaneyoshi, W. Jones, J. Mater. Chem. 9 (1999) 805.
- [17] O.B. Pearson, X. Wu, I. Kustanovich, S.O. Smith, J. Magn. Reson. A 104 (1993) 334.
- [18] W.L. Earl, D.L. VanderHart, J. Magn. Reson. 48 (1982) 35.
- [19] G.R. Williams, A.J. Norquist, D. O'Hare, Chem. Mater. 16 (2004) 975.
- [20] G.R. Williams, D. O'Hare, J. Phys. Chem. B 110 (2006) 10619.
- [21] A.A. Coelho, R.W. Cheary, Programs XFIT and FOURYA, deposited in CCP14 Powder Diffraction Library, Warrington, 1996. <http://www.ccp14.ac.uk/tutorial/xfit-95/xfit.htm>.
- [22] J.D. Hancock, J.H. Sharp, J. Am. Ceram. Soc. 55 (1972) 74.
- [23] S.F. Hulbert, J. Br. Ceram. Soc. 6 (1969) 11.
- [24] K.A. Tarasov, V.P. Isupov, L.E. Chupakhina, D. O'Hare, J. Mater. Chem. 14 (2004) 1443.
- [25] B.J. Teppen, K. Rasmussen, P.M. Bertsch, D.M. Miller, L. Schaefer, J. Phys. Chem. B 101 (1997) 1579.
- [26] F. Belanger-Gariepy, F. Brisse, P.D. Harvey, D.F.R. Gilson, I.S. Butler, Can. J. Chem. 68 (1990) 1163.
- [27] M. Borja, P.K. Dutta, J. Phys. Chem. 96 (1992) 5434.
- [28] O. Ermer, L. Lindenberg, Chem. Ber. 123 (1990) 1111.
- [29] M.J. Hernandez-Moreno, M.A. Ulibarri, J.L. Rendon, C.J. Serna, Phys. Chem. Miner. 12 (1985) 34.
- [30] S. Miyata, Clays Clay Miner. 23 (1975) 369.
- [31] M. Hajek, L. Vodicka, P. Trska, V. Sklenar, Magn. Res. Chem. 23 (1985) 57.